The Topology of Scaffold Routings on Non-Spherical Mesh Wireframes

Abdulmelik Mohammed
Department of Mathematics and Statistics, University of South Florida, Tampa, FL, USA
abdulmelik@usf.edu

Nataša Jonoska
Department of Mathematics and Statistics, University of South Florida, Tampa, FL, USA
jonoska@usf.edu

Masahico Saito
Department of Mathematics and Statistics, University of South Florida, Tampa, FL, USA
saito@usf.edu

Abstract

The routing of a DNA-origami scaffold strand is often modelled as an Eulerian circuit of an Eulerian graph in combinatorial models of DNA origami design. The knot type of the scaffold strand dictates the feasibility of an Eulerian circuit to be used as the scaffold route in the design. Motivated by the topology of scaffold routings in 3D DNA origami, we investigate the knottedness of Eulerian circuits on surface-embedded graphs. We show that certain graph embeddings, checkerboard colorable, always admit unknotted Eulerian circuits. On the other hand, we prove that if a graph admits an embedding in a torus that is not checkerboard colorable, then it can be re-embedded so that all its non-intersecting Eulerian circuits are knotted. For surfaces of genus greater than one, we present an infinite family of checkerboard-colorable graph embeddings where there exist knotted Eulerian circuits.

2012 ACM Subject Classification Mathematics of computing → Discrete mathematics

Keywords and phrases DNA origami, Scaffold routing, Graphs, Surfaces, Knots, Eulerian circuits

Digital Object Identifier 10.4230/LIPIcs.DNA.2020.1

Funding This research was (partially) supported by the grants NSF DMS-1800443/1764366 and the Southeast Center for Mathematics and Biology, an NSF-Simons Research Center for Mathematics of Complex Biological Systems, under National Science Foundation Grant No. DMS-1764406 and Simons Foundation Grant No. 594594. Travel support is provided to Abdulmelik Mohammed through an AMS-Simons Travel Grant (2020).

1 Introduction

The conception of stable branched DNA molecules was one of the central ideas in the birth of DNA nanotechnology [28, 29]. Branched nucleic acids exhibit a mathematical structure naturally modelled by graphs, where graph vertices (roughly points) correspond to the branch locations while graph edges (roughly line segments connecting points) model linear double-helical domains. Graph-theoretic models for the construction of three-dimensional DNA nanostructures have been proposed as early as 1997 [15, 16]. The first experiments demonstrating the self-assembly of non-regular graphs using DNA junctions as vertices and duplexes as edge connectors were presented in 2003 [27]. DNA self assembly has also been used to solve small instances of graph-theoretic problems such as the Directed Hamilton Path problem [2] and the vertex 3-colorability problem [33].

Graphs of convex polyhedra [8, 11, 13, 14, 30] have been synthesized using a variety of DNA vertex and edge motifs. Graph theory took an explicit and integral role in the automated design of non-convex polyhedra when graphs embedded in topological spheres were

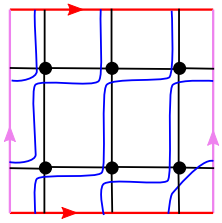

Figure 1 A knotted Eulerian circuit (A-trail) on a torus.

exploited to model a large class of wireframe DNA origami [5, 22]. Thereafter, graph-theoretic modelling has been widely adopted for the design and synthesis of 2D [4, 18, 19] and 3D wireframe DNA origami [17, 32].

In DNA origami [26], a long, typically circular, scaffold strand is folded into a target conformation using hundreds of short helper strands. One of the key and challenging steps in designing complex 3D DNA origami is the routing of the circular scaffold strand so that it covers half the mass of each of the constituent helical domains. In graph based design of DNA origami [5, 4, 32], the scaffold routing typically corresponds to an Eulerian circuit of a graph which has been obtained from the target wireframe after some processing. Briefly, an Eulerian circuit is a closed path in a graph which traces each edge exactly once. Eulerian circuits capture the essential idea that the scaffold constitutes exactly one of the strands in each double helical domain. A general scheme for stapling Eulerian scaffold routings has been proposed in [22].

A fundamental consideration when employing circular strands in the design of nanostructures is ensuring that the topology of the strand routing in the design corresponds to the topology of the physical strand. For instance, the scaffold strand currently used in DNA origami assembly is unknotted. In most DNA origami constructs, the scaffold does not intersect itself when it traces the structure. For this reason, a class of non-intersecting Eulerian circuits called A-trails was adopted for unknotted scaffold routing of Eulerian graphs embedded in a sphere [5]. However, it has been pointed out that A-trails can be knotted for graphs embedded in tori [9]. An example of a knotted A-trail on a torus is shown in Figure 1. The A-trail is illustrated with the blue curve. As usual, the torus is obtained by gluing the horizontal boundaries in red together to form a cylinder and then gluing the violet boundaries to close the cylinder to a torus. Compare with Figure 3 to see that the A-trail corresponds to a trefoil knot. Unknotted scaffold routings may be achieved with non-intersecting Eulerian circuits (a generalization of A-trails, see definitions in Section 2) for graphs that are embedded in surfaces. In this paper, we further investigate the knottedness of non-intersecting Eulerian circuits. These Eulerian circuits can represent knotted or unknotted scaffold routings. Here we specify properties of graph embeddings in surfaces when knotted or unknotted scaffold routings arise from non-intersecting Eulerian circuits.

An approximation algorithm for finding unknotted scaffold routings on triangular embeddings in positive genus surfaces has been proposed earlier [23]. For certain Eulerian graphs, the algorithm can trace some edges twice even if the embedded graph contains an unknotted non-intersecting Eulerian circuit. It has been proved that for checkerboard-colorable graph embeddings (see definition in Section 2) in a torus, A-trails, if any exist, are unknotted [24]. In this paper, we present a number of additional results connecting checkerboard-colorable graph embeddings and the knottedness of non-intersecting Eulerian circuits. We generalize the result of [24] by proving that *all* non-intersecting Eulerian circuits of checkerboard-colorable torus graphs are unknotted. We show that *at least one* unknotted non-intersecting

(a) (b) (c)

Figure 2 Closed orientable surfaces of genus 1, 2 and 3 in (a), (b) and (c), respectively.

Eulerian circuits exists for all checkerboard-colorable embeddings in orientable closed surfaces, including surfaces of genus greater than one. We show that, however, checkerboard-colorable graph embeddings in surfaces of genus greater than one can contain knotted Eulerian circuits. For tori, we characterize graphs which admit embeddings where *all* non-intersecting Eulerian circuits are knotted; such embeddings would require a knotted scaffold for routing as a non-intersecting Eulerian circuit.

2 Preliminaries

Graphs embedded in non-spherical surfaces significantly expand the class of wireframe DNA origami that can be designed based on topological techniques. For instance, reinforced cubes [32] and certain cubic lattices can be modelled as graphs on non-spherical surfaces. In this section, we present the basic topological concepts needed to introduce non-intersecting Eulerian circuits on surface-embedded graphs, our model for topological study of scaffold routings. We refer the reader to Armstrong's book [3] for an accessible account on surfaces, the monograph by Fleischner [10] for a detailed exposition on Eulerian graphs and the first two chapters of Rolfsen's classic [25] for an illustrative introduction to knot theory.

2.1 Surfaces

Surfaces are mathematical models of spaces which, when sufficiently zoomed in, look like a flat plane. Surfaces are commonly used in computer graphics as boundary models of well-defined 3D shapes. The simplest example of a surface is the unit sphere $S^2 = \{(x, y, z) \in \mathbb{R}^3 | x^2 + y^2 + z^2 = 1\}$. Topologically, a sphere is any space homeomorphic to the unit sphere. For instance, the underlying spaces of all the meshes constructed in [5] are topological spheres.

The simplest surface topologically distinct from a sphere is a torus. It is commonly recognized in its standard embedding like the crust of a doughnut (cf. Figure 2a). A torus can be fairly complicated as a geometric figure. The surface of a regular coffee mug is, for instance, topologically a torus. Let S^1 denote the unit circle in the plane. Formally, a *torus* T is a surface homeomorphic to the product space $S^1 \times S^1$. Viewing S^1 as the unit circle in the complex plane, points in a torus can be given coordinates $(e^{i\theta}, e^{i\phi})$, for $0 \leq \theta, \phi < 2\pi$. In the standard embedding of the torus (Figure 2a), θ can be understood as the counter-clockwise rotation with respect to the axis of rotational symmetry, while ϕ denotes the right-handed rotation with respect to the core circle of the embedding. A torus is commonly represented by its fundamental polygon, a square whose parallel edges are identified and glued to form the torus (compare Figure 3c and 3b). On the square, θ can be understood to go from 0 to 2π along the horizontal edge in the positive x direction, while ϕ does so along the vertical edge in the positive y direction.

More complicated surfaces are constructed by joining tori together as follows. The *connected sum* of two surfaces F_1 and F_2 is obtained by removing topological open disks D_i from F_i, for $i \in \{1, 2\}$, and gluing the resulting surfaces $F_i \setminus D_i$ along their boundaries. For instance, the connected sum of two tori is the 2-torus shown in Figure 2b; the blue

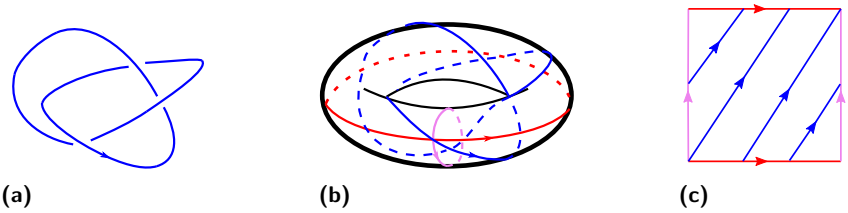

Figure 3 A trefoil knot (a) in a torus (b) and in the fundamental square of the torus (c).

curve indicates the location where the two tori are summed. The classification theorem of (compact, connected, orientable, and without boundary) surfaces states that any surface is either a sphere, a torus, or the connected sum of n tori, for $n \geq 2$. Here, n denotes the *genus* of the surface. The sphere is considered to have genus 0 while the torus has genus 1. As a sample of the classification theorem, three surfaces of genus 1, 2 and 3 are shown in Figure 2a, 2b and 2c, respectively.

A *loop* in a surface F is a continuous map $\beta\colon S^1 \to F$, where S^1 is oriented in this setting, for instance, in the counter-clockwise direction. A loop β is *simple* if $\beta(s_1) \neq \beta(s_2)$, for all pair of distinct points s_1, s_2 in S^1. A simple loop β is said to be *separating* if $F \setminus \mathrm{Im}(\beta)$ consists of two disjoint connected components; otherwise it is *non-separating*. The blue curve in Figure 2b is a separating loop. Two basic examples of non-separating simple loops are the longitude and meridian of the torus, drawn in red and violet in Figure 3b, respectively. The *longitude* of the torus is the loop $\beta_L\colon S^1 \to S^1 \times S^1$ with $\beta_L(e^{i\theta}) = (e^{i\theta}, 1)$, while the *meridian* is the loop $\beta_M\colon S^1 \to S^1 \times S^1$ with $\beta_L(e^{i\phi}) = (1, e^{i\phi})$.

A *knot* is an embedding of the unit circle in $\mathbb{R}^3$. A trefoil knot, which is obtained by joining the two ends of the everyday overhand knot, is illustrated in Figure 3a. Two knots are *equivalent* if there is an orientation preserving self-homeomorphism of $\mathbb{R}^3$ taking the first knot to the second. Intuitively, this represents the fact that two knots are equivalent if and only if the first knot can be continuously deformed to the second one without crossing itself during the deformation. A knot is *trivial* or an *unknot* if it is equivalent to the unit circle in the plane. Otherwise it is *non-trivial*. A knot is trivial if and only if it bounds a disk (tamely) embedded in $\mathbb{R}^3$ (see Theorem 10.6, p. 224 in [3]).

A *torus knot* is a non-trivial knot that lies in the standard torus. As the sketch in Figure 3b demonstrates, the trefoil knot is a torus knot; Figure 3c depicts the knot in the fundamental square of the torus. Loops on the torus belong to homotopy classes that can be identified by a pair of integers (a, b), where a denotes the number of times the loop goes around in the positive longitude direction and b denotes the number of times it goes around the positive meridian direction. A class (a, b) is represented by a simple loop if and only if both a and b are zero, or $gcd(a, b) = 1$ [25, p. 19]. A simple loop on a torus is a trivial knot if $|a| \leq 1$ or $|b| \leq 1$; otherwise, it is a non-trivial knot. Thus, torus knots can be identified with a pair of coprime integers (a, b) with absolute values greater than one. The trefoil knot shown in Figure 3a is a torus knot of type $(2, 3)$.

A *longitudinal (Dehn) twist* of a torus is a self-homeomorphism $h_L\colon T \to T$ with $h((e^{i\theta}, e^{i\phi})) = (e^{i(\theta+\phi)}, e^{i\phi})$. A *meridional (Dehn) twist* is a self-homeomorphism $h_M\colon T \to T$ with $h((e^{i\theta}, e^{i\phi})) = (e^{i\phi}, e^{i(\phi+\theta)})$. It is to be understood that h_L and h_M constitute positive twists while their inverses form negative twists. Intuitively, a longitudinal (resp. meridional) twist is obtained by cutting the torus along the longitude (resp. meridian), twisting the resulting cylinder by 360° and gluing the cylinder ends together to form a torus. On the fundamental square of the torus, a longitudinal twist can be visualized as a horizontal shear,

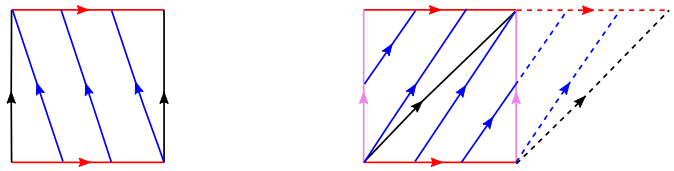

Figure 4 A longitudinal twist of a torus sending a $(-1, 3)$ loop in a torus (a) to the $(2, 3)$ torus knot (b).

as illustrated in Figure 4; the upper triangle protruding from the square is to be understood as coming back on the left to join with the lower triangle. A meridional twist can analogously be visualized as a vertical shear of the square. A positive longitudinal twist maps a knot of class (a, b) to a knot of class $(a + b, b)$ while a positive meridional twist maps a knot of class (a, b) to a knot of class $(a, a + b)$ [25, p. 24]. Negative twists map from class (a, b) to classes $(a - b, b)$ and $(a, -a + b)$, respectively. A positive longitudinal twist taking a $(-3, 1)$ unknot to the $(2, 3)$ trefoil knot is shown in Figure 4; Figure 4a shows the unknot, while the trefoil knot that is produced by the twist is shown in Figure 4b.

2.2 Graphs

Graphs are natural models to represent the branching of nucleic acids and have been successfully used to design DNA origami polyhedral wireframes [5, 32]. While a surface models the set of all points in the boundary of a polyhedron, the wireframe composed of the corners and edges of a polyhedron constitute the graph that is embedded in the surface. Here, we briefly recall some basic notions related to graphs. We refer the reader to [12] for a thorough but accessible introduction to graphs on surfaces.

All graphs under consideration in this paper are finite and undirected but, for brevity of construction, can contain multiedges and loops. It is assumed that all graphs contain at least one edge. Each edge in a graph is understood to be composed of two half edges which are incident to the two endpoints of the edge; in the case of a loop edge, the two half edges meet the same vertex. The degree of a vertex v is the number of half edges incident to it and is denoted by $d(v)$. A vertex is said to be *even* if it has an even degree.

For graphs that are embedded in surfaces, it is convenient to think of graphs as topological spaces which are endowed a 1-dimensional cell structure, where the 0-cells correspond to vertices and the 1-cells correspond to edges. An *embedding* $g\colon G \to F$ of a graph G in a surface F is a topological embedding of G into F; that is, the image $g(G)$ is homeomorphic to the topological space G. In other terms, an embedding of a graph is a drawing of the graph on the surface where no edges cross. The space $F \setminus g(G)$ consists of disjoint connected subspaces called *faces*. An embedding of a graph in a surface is said to be *checkerboard colorable* if the faces can be assigned two colors (e.g. black and white) such that, for every edge, the two faces on the two sides of the edge are assigned distinct colors; if there is an edge where one face is present on both sides of the edge, the embedding is not checkerboard colorable. See Figure 8a for a checkerboard-colorable embedding of K_7, the complete graph on seven vertices.

An embedding $g\colon G \to F$ is said to be *cellular* if each face is homeomorphic to the open unit disk. A cellular embedding of a simple graph is said to be *triangular* if each face is bounded by three distinct edges. An embedding $g\colon G \to F$ determines a counter-clockwise cyclic order ρ_v of the half edges incident at a vertex v, for each vertex v in the graph. The

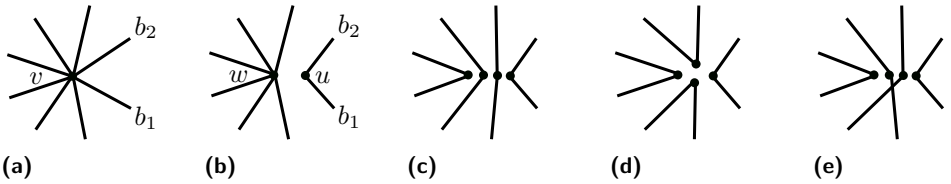

Figure 5 Smoothing of an even vertex. (a) Neighboring half edges in a vertex, (b) smoothing one transition composed of the neighboring half edges, (c) a smoothing of the vertex induced by a non-intersecting Eulerian circuit, (d) a smoothing induced by an A-trail, (e) a splitting away of transitions where two transitions intersect.

order ρ_v is called a *rotation* at v. The collection $\rho = \{\rho_v : v \in G\}$ of rotations at vertices is called a *rotation system*. In a rotation system, each vertex can be treated as rigid (see [7] for the notion of rigid vertices). Conversely, if each vertex is rigid, it gives rise to a cellular embedding $g : G \to F$ for some (closed orientable) surface F.

In wireframe DNA origami [5, 32], the fact that the scaffold comprises one strand of each double-helical domain is conveniently captured by an Eulerian circuit of an underlying graph. A *circuit* in a graph is a closed walk $(v_0, e_0, v_1, \ldots, v_{l-1}, e_{l-1}, v_0)$ with no repeated edges, where $l \geq 1$ is the *length* of the circuit and each e_i, for $0 \leq i \leq l-1$, is an edge in the graph with endpoints v_i, $v_{i+1 \bmod l}$. An *Eulerian circuit* is a circuit which visits every edge of the graph. A graph is said to be *Eulerian* if it contains an Eulerian circuit. A connected graph is Eulerian if and only if every vertex is of even degree. Closely related to circuits are cycles and transitions. A *cycle* is a circuit with no repeated vertices. For a surface-embedded graph, a cycle corresponds to a simple loop and the separating/non-separating qualification equally apply to cycles. A *transition* is an unordered pair of half edges incident to a common vertex. A circuit $C = (v_0, e_0, v_1, \ldots, v_{l-1}, e_{l-1}, v_0)$ can also be seen as a collection of transitions $\{b_i, b'_{i+1 \bmod l}\}$, where b_i is the half edge of e_i incident to $v_{i+1 \bmod l}$, and b'_i is the half edge of e_i incident with v_i, for all $i \in \{0, \ldots, l-l\}$. In this sense, we can say that $\{b_i, b'_{i+1 \bmod l}\}$ is contained in C.

Let $g : G \to F$ be an embedding of a graph in a surface. Let v be a vertex of G with $d(v) \geq 4$ and let the rotation ρ_v determined by g be $(b_0, \ldots, b_{d(v)-1})$. Let $0 \leq i, j, k, l \leq d(v) - 1$ with $i < j, k < l, i < k$. A pair of disjoint transitions $\{b_i, b_j\}$, $\{b_k, b_l\}$ *intersect* if $i < k < j < l$ (cf. Figure 5e). An Eulerian circuit of an Eulerian graph G is said to be *non-intersecting* with respect to $g : G \to F$ if it contains no intersecting transitions with respect to g (cf. the collection of transitions of the vertex v in Figure 5a suggested by Figure 5c). It has been shown that a non-intersecting Eulerian circuit can be found in polynomial time for any Eulerian graph embedded in a sphere [1, 31], or in any other surface [10, 23]. However, the computational complexity changes when considering a subclass of non-intersecting Eulerian circuits called A-trails. Two half edges b_1, b_2 incident to a vertex v are said to be *neighbors* if $\rho_v(b_1) = b_2$ or $\rho_v(b_2) = b_1$ (see Figure 5a for an example). An *A-trail* is a non-intersecting Eulerian circuit where every transition is composed of neighboring half edges (cf. Figure 5d). Deciding whether a surface-embedded graph has an A-trail is known to be NP-COMPLETE, even when restricted to embeddings in a sphere [6].

Let $g : G \to F$ be a graph embedded in a surface. Let v be a vertex of G, $d(v) \geq 4$, with rotation ρ_v determined by g. Let $t = \{b_1, b_2\}$ be a transition composed of neighboring half edges incident to v. A *smoothing of a transition* t is the graph embedded in F obtained from (G, g) by deleting v and adding two new vertices u and w such that b_1 and b_2 become incident with u and the rest of the half edges become incident with w. The graph obtained

after smoothing is embedded exactly according to g except in a local disk neighborhood of v where u and w are embedded in a manner illustrated by the example in Figure 5b. Note that the two half edges flanking b_1 and b_2 become neighbors in the new embedding. The notion of smoothing defined here is a special case of the notion of "splitting away a pair of edges" [10, p. III.16] catered to non-intersecting Eulerian circuits. Now suppose v is even and its incident half edges are partitioned into disjoint mutually non-intersecting transitions. The transitions can be ordered as $\sigma = (t_1, \ldots, t_{d(v)/2})$ such that t_1 is composed of neighboring half edges, and each t_{i+1} is composed of neighboring half edges after t_i has been smoothed. A *smoothing of* v is the embedded graph $\tilde{g}_v \colon \tilde{G}_v \to F$ obtained after such a sequence σ of smoothings of transitions. Two possible smoothings of the vertex v in Figure 5a are shown in Figures 5c and 5d. We note that smoothings of a vertex are in bijection with crossingless chord diagrams. The number of possible smoothings of a vertex v is the Catalan number $C_k = \frac{1}{k+1}\binom{2k}{k}$, where $k = \frac{d(v)}{2}$. A *smoothing of a non-intersecting Eulerian circuit* γ is the embedded cycle graph $\tilde{\gamma}$ obtained after smoothing all the vertices according to the transitions in γ. The smoothed Eulerian circuit $\tilde{\gamma}$ is unique up to isotopy. Figures 5c and 5d illustrate smoothings of a vertex based on a non-intersecting Eulerian circuit and an A-trail, respectively.

Having established the concepts, the general scheme of discussion is as follows: we are given an Eulerian graph G embedded in a surface F and a non-intersecting Eulerian circuit γ; then F is embedded in $\mathbb{R}^3$. In notation, this is described as: $\gamma \to G \overset{g}{\hookrightarrow} F \overset{f}{\hookrightarrow} \mathbb{R}^3$.

We then ask whether $f(\tilde{\gamma})$ is an unknot or a non-trivial knot. We present results where $f(\tilde{\gamma})$ is an unknot in Section 3 and results where $f(\tilde{\gamma})$ is a non-trivial knot in Section 4. When $f(\tilde{\gamma})$ is an unknot, the regular unknotted scaffold can be routed according to γ; otherwise either a knotted scaffold must be used, or a different unknotted non-intersecting Eulerian circuit must be chosen. If all $f(\tilde{\gamma})$ are non-trivial knots, a knotted scaffold is necessary for routing the embedded graph using a non-intersecting Eulerian circuit.

3 Unknotted Scaffold Routings

When the available scaffold is unknotted, as typically is the case, we aim to find unknotted non-intersecting Eulerian circuits. In this section, we show that checkerboard colorability of an embedding is a sufficient condition for an embedded graph to contain an unknotted non-intersecting Eulerian circuit, thus allowing design using the typical unknotted scaffold strand.

It is well-known that a graph embedded in a sphere is Eulerian if and only if the embedding is checkerboard colorable [10, Theorem III.68]. Although an Eulerian graph embedded in a positive genus surface may not be checkerboard colorable, we show that checkerboard colorability affects the topology of Eulerian circuits on surface-embedded graphs. It has been shown that [24, Theorem 3.6] all A-trails (if any exist) on checkerboard-colorable torus graphs are unknotted, for any embedding $f \colon T \to \mathbb{R}^3$. We first generalize this result to all non-intersecting Eulerian circuits using a more topological proof. We then show a general result for all surfaces: every checkerboard-colorable surface-embedded graph admits an unknotted non-intersecting Eulerian circuit.

Non-intersecting Eulerian circuits are unknotted on a sphere due to the Jordan-Schönflies theorem [25, p. 9], which states that every simple loop in a sphere is separating and bounds a disk. On the other hand, simple loops in a torus can either be separating or non-separating. A separating loop in a torus bounds a disk on one side and thus one strategy to find an unknotted non-intersecting Eulerian circuit on a torus graph is to search for a separating non-intersecting Eulerian circuit. In Lemma 2, we show that the checkerboard colorability

Figure 6 A checkerboard coloring viewed locally at a vertex (a) and how it induces a checkerboard coloring when the vertex is smoothed (b).

of a graph embedding is a sufficient criteria for its non-intersecting Eulerian circuits to be separating. To prove Lemma 2, we first prove in Lemma 1 that checkerboard colorability is preserved under smoothing and unsmoothing of vertices.

▶ **Lemma 1.** *Let $g\colon G \to F$ be an embedding of an Eulerian graph G in a surface F and let $\tilde{g}_v\colon \tilde{G}_v \to F$ be an embedding obtained by smoothing a vertex v of G. Then, g is checkerboard colorable if and only if $\tilde{g}_v$ is checkerboard colorable.*

Proof. The proof idea is sufficiently illustrated by the example in Figure 6, where a checkerboard coloring of g (Figure 6a) is extended to a checkerboard coloring of $\tilde{g}_v$ (Figure 6b). In words, since any smoothing of v is by definition obtained as a sequence of smoothings of transitions (composed of neighboring edges), it is sufficient to prove the claim for a smoothing of a transition. In a checkerboard coloring, if the faces that merge when smoothing a transition are distinct, they are colored alike before they merge. In this manner, a checkerboard coloring of g extends to a checkerboard coloring of $\tilde{g}_v$ when the faces are merged. When unsmoothing a transition, if a face is split into two faces, the new faces inherit the color of the parent for a checkerboard coloring of the new embedding. In this way, a checkerboard coloring of $\tilde{g}_v$ naturally induces a checkerboard coloring of g. ◀

We can now prove Lemma 2 that relates checkerboard colorability of graph embeddings and the separating property of non-intersecting Eulerian circuits.

▶ **Lemma 2.** *Let $g\colon G \to F$ be an embedding of an Eulerian graph G in a surface F. The following claims hold for every smoothed non-intersecting Eulerian circuit $\tilde{\gamma}$ of (G, g):*

(i) *If g is checkerboard colorable, then $\tilde{\gamma}$ is separating;*

(ii) *If g is not checkerboard colorable, then $\tilde{\gamma}$ is non-separating.*

Proof. **(i)** Let γ be an arbitrary non-intersecting Eulerian circuit of (G, g). If g is checkerboard colorable, then $\tilde{\gamma}$ is checkerboard colorable by Lemma 1. In a checkerboard coloring of $\tilde{\gamma}$ the two sides of $\tilde{\gamma}$ must be colored differently; thus the two sides must be in distinct faces and $\tilde{\gamma}$ must be separating.

(ii) By the contrapositive, suppose there exists a separating smoothed non-intersecting Eulerian circuit $\tilde{\gamma}$. Since $\tilde{\gamma}$ is separating, the two separate regions can be colored distinctly to obtain a checkerboard coloring of $\tilde{\gamma}$. By Lemma 1, unsmoothing $\tilde{\gamma}$ to g gives rise to a checkerboard coloring of g. ◀

Lemma 2 equips us to generalize Theorem 3.6 of [24] to non-intersecting Eulerian circuits on checkerboard-colorable torus graphs, as stated in Theorem 3.

▶ **Theorem 3.** *If $g\colon G \to T$ is a checkerboard-colorable cellular embedding of an Eulerian graph in a torus, then $f(\tilde{\gamma})$ is an unknot for any non-intersecting Eulerian circuit γ of (G, g) and any embedding $f\colon T \to \mathbb{R}^3$.*

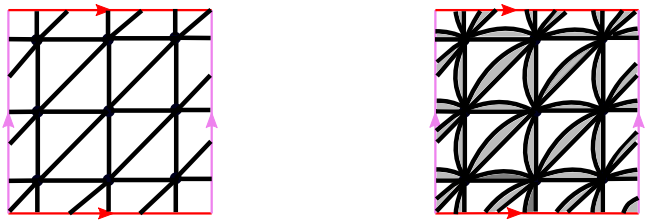

Figure 7 A checkerboard-colorable graph embedding (b) obtained by doubling the edges of a graph which has a triangular embedding in a torus (a).

Proof. By Lemma 2, any smoothed non-intersected Eulerian circuit $\tilde{\gamma}$ of (G, g) is separating. A separating loop in a torus bounds a disk and thus $\tilde{\gamma}$ bounds a disk. Under any homeomorphism of T, $\tilde{\gamma}$ still bounds a disk and thus $f(\tilde{\gamma})$ is an unknot for any embedding $f\colon T \to \mathbb{R}^3$ of the torus in $\mathbb{R}^3$. ◀

For checkerboard-colorable embeddings on a torus, by Theorem 3, *any* non-intersecting Eulerian circuit can be used as a route for an unknotted scaffold strand. Theorem 3 suggests the existence of graphs where the unknottedness of non-intersecting Eulerian circuits can be guaranteed purely from the adjacency structure of the abstract graph, i.e., independent of the graph embedding in the torus and of the torus' embedding in $\mathbb{R}^3$. An infinite family of graphs with this property is presented in Proposition 4. For such families of graphs, the possibility of routing using unknotted scaffold strand is completely determined from the abstract graph.

▶ **Proposition 4.** *There exist an infinite family $\mathcal{G}$ of Eulerian graphs such that for all $G \in \mathcal{G}$, and all $g\colon G \to T$, and all $f\colon T \to \mathbb{R}^3$, and all non-intersecting Eulerian circuit γ of (G, g), $f(\tilde{\gamma})$ is an unknot.*

Proof. Let $\mathcal{G}$ be the family of graphs obtained by doubling the edges of graphs with triangular embedding in a torus. Let G be a graph in $\mathcal{G}$. One example is shown in Figure 7b. Consider any pair e_1, e_2 of double edges with endpoints u and v. With slight abuse of notation, let ρ_u (resp. ρ_v) denote the cyclic counter-clockwise order of the edges, instead of half edges, incident with u (resp. v). In any embedding g of G in a torus, either $\rho_u(e_1) = e_2$ or $\rho_u(e_2) = e_1$. If $\rho_u(e_1) = e_2$ then $\rho_v(e_2) = e_1$; otherwise $\rho_v(e_1) = e_2$. Thus, double edges such as e_1, e_2 bound faces in g. These faces can be shaded black, while the other faces are left white, to get a checkerboard coloring of g (cf. Figure 7b). The claim then follows from Theorem 3. ◀

Theorem 3 crucially depends on the surface being a torus, as a separating loop in a surface of genus greater than one need not bound a disk. For instance, the blue loop in the double torus in Figure 2b is separating but bounds punctured tori on both sides. In Section 4 (Theorem 8), we employ this property to construct families of checkerboard-colorable embeddings in F_n ($n \geq 2$) with knotted non-intersecting Eulerian circuits. Although checkerboard colorability is not sufficient to guarantee that *all* non-intersecting Eulerian circuits are unknotted for embeddings in surfaces of genus at least two, it is sufficient to ensure that there is *at least one* unknotted non-intersecting Eulerian circuit, as shown in Theorem 5. Thus, checkerboard-colorable graph embeddings can generally be routed using an unknotted scaffold.

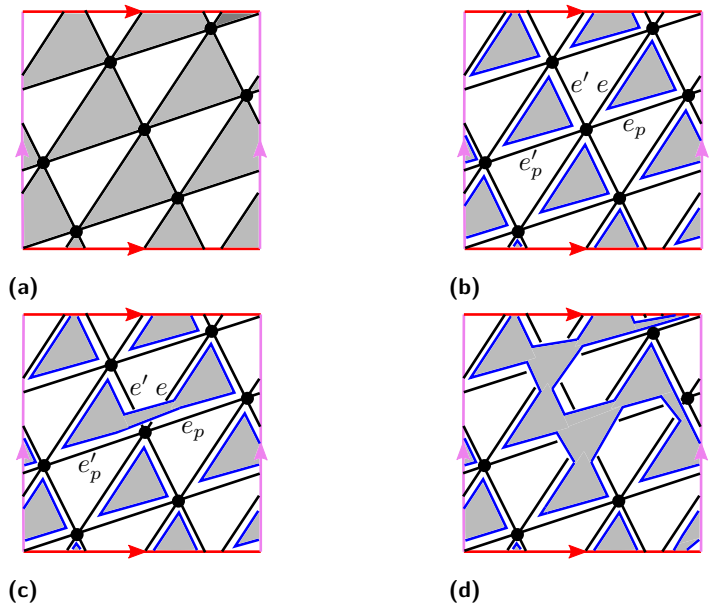

Figure 8 An unknotted non-intersecting Eulerian circuit of K_7 in a torus. (a) a checkerboard-colorable embedding of K_7 in a torus, (b) circuits bounding the black faces, (c) merging circuits, (d) the unknotted non-intersecting Eulerian circuit.

▶ **Theorem 5.** *If $g\colon G \to F$ is a checkerboard-colorable cellular embedding of an Eulerian graph G in a surface F, then there exists a non-intersecting Eulerian circuit γ of G such that $f(\tilde{\gamma})$ is unknotted for any embedding $f\colon F \to \mathbb{R}^3$.*

Proof. Let $g\colon G \to F$ be a checkerboard-colorable embedding of an Eulerian graph in a surface F. An example is given by the embedding of K_7 in the torus shown in Figure 8a. Let the faces of g be colored with black and white. By the definition of checkerboard coloring, each edge is incident to exactly one black face and one white face. Thus, the collection of all the boundary circuits of the black faces form a non-intersecting circuit partition of G. Because the embedding is cellular, the circuits bound disjoint closed disks after a small isotopy. This is illustrated in Figure 8b for the embedding of K_7 in a torus.

To convert the non-intersecting circuit partition into a non-intersecting Eulerian circuit γ, we perform a re-splicing of disjoint circuits one by one at each vertex (see Lemma 7 of [23] for details). We go through the edges incident to the vertex in the cyclic order they appear in the embedding, and if two neighboring edges e and e' are not in the same circuit, we re-splice the two circuits so that e and e' are paired to each other and e's previous pair e_p is paired with e''s previous pair e'_p (cf. Figure 8c). This re-pairing merges the two circuits and reduces the number of circuits in the circuit partition, while keeping the circuit partition non-intersecting. A repeated application of this operation for every vertex in the graph yields a non-intersecting Eulerian circuit γ.

Now consider any embedding $f\colon F \to \mathbb{R}^3$. To prove $f(\tilde{\gamma})$ is an unknot, we show by induction that $\tilde{\gamma}$ bounds a disk. In particular, we prove that, after each merge of circuits through a re-pairing of edges, each circuit in the circuit partition, up to isotopy, bounds a closed disk. The base case is handled by the circuit partition formed from the black faces. Suppose by induction hypothesis that all the circuits before the pairing of e and e' bound a disk. The re-pairing joins the two disjoint disks by a band, which results in a new disk that the new circuit bounds (cf. Figure 8c). For the embedding of K_7 in a torus, the non-intersecting Eulerian circuit, and the disk that it bounds can be seen in Figure 8d. ◀

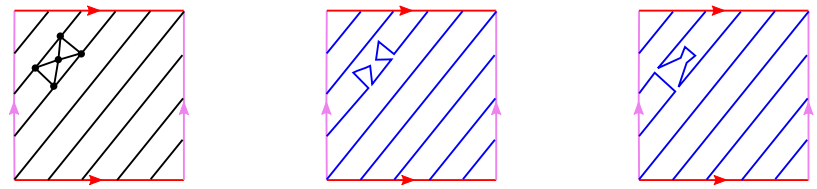

Figure 9 Knotted Eulerian circuits on an embedding of K_5 in the torus. (a) an embedding of K_5 in a torus, (b) a non-intersecting Eulerian circuit which is a $(4, 5)$ torus knot, (c) a non-intersecting Eulerian circuit which is a $(2, 3)$ torus knot.

4 Knotted Scaffold Routings

In Section 3, we saw that checkerboard-colorable embeddings are closely related to the existence of unknotted scaffold routings. In this section, we study the relationship between non-checkerboard colorable embeddings and the existence of knotted scaffold routings.

A non-intersecting Eulerian circuit γ on a surface-embedded graph can be knotted due to the embedding g of the graph in the surface or due to the embedding f of the surface in $\mathbb{R}^3$. Moreover, $f(\tilde{\gamma})$ can be either an unknot or a non-trivial knot for a fixed embedding g, depending on f. For instance, consider the Eulerian graph B formed by the crossing of the meridian and longitude of the torus. That is, B is the bouquet of two circles with one vertex and two loop edges and its embedding g is the natural one where the vertex is placed at the crossing point of the meridian and longitude (recall Figure 3b). Note that B has two Eulerian circuits which have identical structure; let γ be one of these circuits. In a standard embedding of the torus (Figure 3b), $f(\tilde{\gamma})$ is an unknot. However, if the torus is embedded in $\mathbb{R}^3$ as a tubular neighborhood of a non-trivial knot K such that the longitude is equivalent to K, then $f(\tilde{\gamma})$ is also equivalent to K and thus non-trivial. The construction generalizes to graph embeddings that are not checkerboard colorable, in the sense described in Theorem 6.

▶ **Theorem 6.** *Suppose $g : G \to F$ is an embedding of an Eulerian graph G in a surface F and suppose that g is not checkerboard colorable. Then, for any non-intersecting Eulerian circuit γ, there exists an embedding $f : F \to \mathbb{R}^3$ such that $f(\tilde{\gamma})$ is a non-trivial knot.*

Proof. Let $g : G \to F$ be an embedding that is not checkerboard colorable, and γ be a non-intersecting Eulerian circuit. By Lemma 2, $\tilde{\gamma}$ is a non-separating loop in F. Hence, after applying a homeomorphism of F, $\tilde{\gamma}$ can be considered to be positioned as a *longitudinal* loop in F (a curve that goes around a hole, just like a longitude of a torus). Then we can choose an embedding $f : F \to \mathbb{R}^3$ such that this longitudinal loop $\tilde{\gamma}$ is knotted.

The observation above, taking $\tilde{\gamma}$ as longitudinal as a consequence of g being not checkerboard colorable, can be deduced using the first homology groups in homology theory; here the technical details are omitted. ◀

We now focus on the case where the embedding of the surface is standard. It has been shown that the bouquet of two circles can be embedded in a standard torus so that all the non-intersecting Eulerian circuits are knotted [24, Figure 11]. Figure 9a shows an embedding of the toroidal graph K_5 where all its non-intersecting Eulerian circuits are knotted. A non-intersecting Eulerian circuit of this embedding of K_5 is either a $(4, 5)$ torus knot (e.g. Figure 9b) or a $(2, 3)$ torus knot (e.g. Figure 9c). Theorem 7 characterizes Eulerian graphs which admit toroidal embeddings where all the non-intersecting Eulerian circuits are knotted.

Theorem 7 shows the existence of embeddings of Eulerian graphs where a routing as a non-intersecting Eulerian circuit would necessitate the use of knotted scaffold strands. It also supports the suggestion in [9] that knotted scaffolds could expand the possible set of DNA origami meshes that can be constructed.

▶ **Theorem 7.** *An Eulerian graph admits a cellular embedding in a standardly embedded torus where all smoothed non-intersecting Eulerian circuits are knotted if and only if it admits a cellular embedding in a torus that is not checkerboard colorable.*

Proof. ($\implies$) By the contrapositive, if all the embeddings of a graph in a torus are checkerboard colorable, then by Theorem 3, each of these embeddings will contain an unknotted non-intersecting Eulerian circuit.

($\impliedby$) Let $g\colon G \to T$ be a cellular embedding of an Eulerian graph in a torus such that the embedding is not checkerboard colorable. The main idea of the proof is to use self-homeomorphisms of the torus to twist g so that each of the non-intersecting circuits becomes a non-trivial knot when the torus is embedded in a standard fashion in $\mathbb{R}^3$. This is possible because the number of non-intersecting Eulerian circuits is finite and each smoothed non-intersecting Eulerian circuit is non-separating (Lemma 2). A concrete combination of twists is presented next.

Since every (smoothed) non-intersecting Eulerian circuit of (G, g) is non-separating, each oriented non-intersecting Eulerian circuit can be represented by a pair (a, b) of integers with $(a, b) \neq (0, 0)$ and $gcd(a, b) = 1$. Let the ith oriented non-intersecting Eulerian circuit (in some order) be represented with (a_i, b_i). Let k, l, m be natural numbers representing the twists that are to be determined. Applying k longitudinal twists to T converts the embedding g to an embedding g_1 so that the Eulerian circuits become simple loops of type $(a_i + kb_i, b_i)$. Next, applying l meridional twists converts g_1 to an embedding g_2 so that the circuits become simple loops of type $(a_i + kb_i, la_i + (lk + 1)b_i)$. Finally, applying m longitudinal twists converts g_2 to an embedding g_3 so that the circuits are simple loops of type $((1 + lm)a_i + (k + mlk + m)b_i), la_i + (k + 1)b_i))$. We thus only need to choose k, l, m so that $|(1 + lm)a_i + (k + mlk + m)b_i)| > 1$ and $|la_i + (k + 1)b_i)| > 1$, for all i; that is, k, l, m are to be chosen so that all the circuits become non-trivial knots. For this purpose, we can choose $l = 2, m = 1$ and $k = \max_{i:b_i \neq 0}\{\frac{2|a_i|}{|b_i|} + 1\}$ if there exists a $b_i \neq 0$, or $k = 1$ if $b_i = 0$ for all i. Since $(a_i, b_i) \neq (0, 0)$, we need to consider three cases:

- **(i)** $a_i = 0$ and $b_i \neq 0$. Then, $|(1 + lm)a_i + (k + mlk + m)b_i)| = |(3k + 1)b_i| = (3k + 1)|b_i| \geq (6\frac{|a_i|}{|b_i|} + 4)|b_i| = 4|b_i| \geq 4$. Additionally, $|la_i + (k + 1)b_i)| = |(k + 1)b_i| = (k + 1)|b_i| \geq (\frac{2|a_i|}{|b_i|} + 2)|b_i| \geq 2$.
- **(ii)** $a_i \neq 0$ and $b_i = 0$. Then $|(1 + lm)a_i + (k + mlk + m)b_i)| = 3|a_i| \geq 3$. Moreover, $|la_i + (k + 1)b_i)| = 2|a_i| \geq 2$.
- **(iii)** $a_i \neq 0$ and $b_i \neq 0$. Then $|(1 + lm)a_i + (k + mlk + m)b_i)| = |3a_i + (3k + 1)b_i| \geq |(3k + 1)b_i| - |3a_i| = (3k + 1)|b_i| - |3a_i| \geq (6\frac{|a_i|}{|b_i|} + 4)|b_i| - 3|a_i| = 3|a_i| + 4|b_i| \geq 7$. And $|la_i + (k + 1)b_i)| = |2a_i + (k + 1)b_i| \geq |(k + 1)b_i| - |2a_i| = (k + 1)|b_i| - |2a_i| \geq (\frac{2|a_i|}{|b_i|} + 2)|b_i| - 2|a_i| = 2|b_i| \geq 2$. ◀

Note that the twists in the proof of Theorem 7 need not change the rotation system determined by the embedding. This highlights the geometric nature of the problem, in the sense that the existence of knotted non-intersecting Eulerian circuits cannot generally be completely determined from the combinatorial structure of the embedding. In fact, the original embedding g may have no knotted non-intersecting Eulerian circuits at all, as is the case for instance, with the standard embedding of the bouquet of two circles in the standard torus. Nevertheless, Theorem 7 provides a mechanism to check whether an

Eulerian graph admits an embedding in a torus where all the non-intersecting Eulerian circuits are knotted, as one can algorithmically determine whether a graph admits a cellular embedding in a torus that is not checkerboard colorable. Indeed, this can be done by going through the finite number of possible rotation systems of the graph, obtaining the cellular embeddings corresponding to the rotation systems via standard face-tracing algorithms in topological graph theory [12, p. 115], checking that the embedding is in a torus from the generalized Euler's polyhedron formula [12, p. 27, p. 122], and then checking for checkerboard colorability. Determining checkerboard colorability of a cellular embedding is equivalent to deciding whether the geometric dual is bipartite, which can be done through a standard breadth-first-search algorithm.

For surfaces of genus greater than one, even checkerboard-colorable embeddings can have knotted non-intersecting Eulerian circuits, as demonstrated by the infinite family in Theorem 8. Note that in Theorem 8, the claim is not that *all* non-intersecting Eulerian circuits are knotted but that there is *at least one* that is knotted. The problem of characterizing graphs which admit cellular embeddings in a standardly embedded surface F_n, $n \geq 2$, so that all non-intersecting Eulerian circuits are knotted is left for future work. Theorem 8 suggests that, unlike the case of the torus, checkerboard-colorable embeddings of graphs in surfaces of genus larger than one can possibly be routed and constructed using knotted scaffold strands.

▶ **Theorem 8.** *Let F_n be an orientable closed surface of genus n that is standardly embedded in $\mathbb{R}^3$.*

- **(i)** *For all $n \geq 2$, there exist infinitely many Eulerian graphs that have checkerboard-colorable cellular embeddings in F_n with knotted non-intersecting Eulerian circuits.*
- **(ii)** *For any non-trivial knot K, there exists an Eulerian graph G cellularly embedded with a checkerboard coloring in F_n for some $n \geq 1$ having K as a non-intersecting Eulerian circuit of G.*

Proof. First consider the case $n = 2$ for (i). Let S be an orientable surface with a connected boundary obtained from a disk by attaching two twisted unknotted bands. An example is depicted in Figure 10. The twists must be full (versus half) twists to obtain an orientable surface. The boundary ∂S of S is a non-trivial knot K.

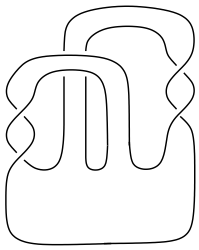

Figure 10 Two twisted bands attached to a disk.

Let $F = F_n$ $(n = 2)$ be the surface obtained by thickening S. Figure 11 depicts this process. In Figure 11a a portion of a band is depicted. The top image of Figure 11a is a cross sectional view of a part of a band depicted at the bottom. In Figure 11b a thickened band is depicted with its cross section shown at the top. The boundary after thickening is a tube. By applying this process to S, we obtain a standard surface F as depicted in Figure 12. The knot K can be regarded as staying on F as in Figure 12, indicated by a red curve. Note that K divides F into two parts (in Figure 11b the two parts are the front and back faces).

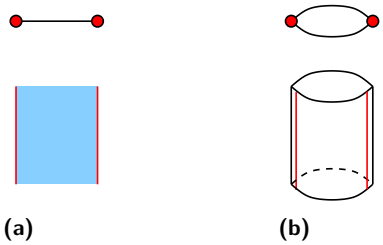

Figure 11 Thickening a band (a) to a tube (b).

Next we construct a graph G cellularly embedded in F by *finger moves* as depicted in Figure 13. In Figure 13a, a dotted arc connects two parts of K. Push one end of K along the arc, and at the other end make it intersect in two double points as indicated in Figure 13b. After one finger move we obtain a 4-regular graph with two vertices. In Figure 14, it is shown that a finger move preserves the checkerboard colorability as in Figure 14b, and there is a choice of a non-intersecting Eulerian circuit that is the original knot K as illustrated in Figure 14c by a blue curve. By repeating finger moves across non-cellular faces, we obtain a cellularly embedded graph G with K as a non-intersecting Eulerian circuit.

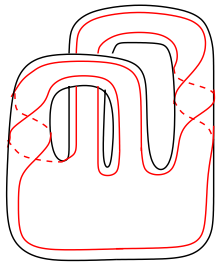

Figure 12 The boundary surface after thickening contains the original knot.

This construction can be performed for any even $n \in \mathbb{N}$. For an odd n, we add a trivial handle to F_{n-1} as indicated in Figure 15a. At this point G becomes non-cellular. To obtain a new cellularly embedded graph, we perform two finger moves as depicted in Figure 15b. The new graph retains the checkerboard colorability and the property of having K as a non-intersecting Eulerian circuit, as desired. The construction allows for infinitely many such graphs, for example by performing additional finger moves, or by choosing different arcs for finger moves. This completes the proof of (i).

Figure 13 A finger move (b) along a dotted arc (a).

(ii) It is known that any knot K can be realized as the boundary of an orientable surface S, such that a thickened S is a standard handlebody. Hence a similar argument applies. ◀

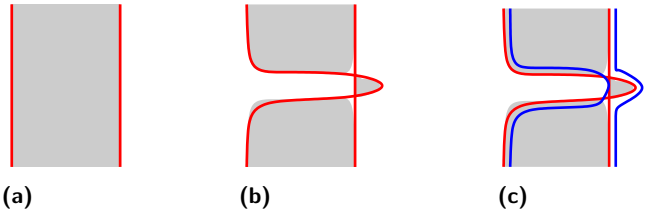

Figure 14 A checkerboard coloring before (a) and after a finger move (b). A choice of non-intersecting Eulerian circuit after a finger move (c).

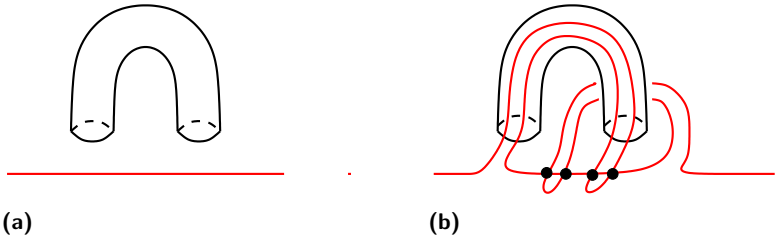

Figure 15 A handle added to make the genus odd (a) and finger moves to make the embedding cellular (b).

5 Conclusion

Eulerian circuits are emerging as broadly applicable model of strand routings in biomolecular technology [4, 5, 20, 21, 32]. For circular strands, the knot type of the strand routing in the design must conform to the knot type of the strand in solution. Herein, we studied the knottedness of strand routings modelled by non-intersecting Eulerian circuits of Eulerian graphs embedded in surfaces.

We showed a strong connection between checkerboard-colorable graph embeddings in surfaces and the knottedness of non-intersecting Eulerian circuits. We extended the result of [24] by showing that all non-intersecting Eulerian circuits are unknotted for checkerboard-colorable torus graphs (Theorem 3). Thus, checkerboard-colorable torus graphs can be routed (as non-intersecting Eulerian circuits) using unknotted scaffolds but they cannot be routed using knotted ones. For checkerboard-colorable embeddings in surfaces of genus greater than one, we showed that there is at least one unknotted non-intersecting Eulerian circuit (Theorem 5). Thus, all checkerboard-colorable graph embeddings can be routed using unknotted scaffold strands. We proved that checkerboard-colorable embedded graphs in surfaces of genus greater than one can have knotted Eulerian circuits (Theorem 8) and hence knotted scaffolds can potentially be used to construct checkerboard colorable graph embeddings in non-toroidal (and non-spherical) surfaces. For torus graphs, we characterized Eulerian graphs which admit an embedding in a standard torus where all non-intersecting Eulerian circuits are knotted. These are precisely the Eulerian graphs which admit embeddings in a torus that are not checkerboard colorable (Theorem 7). This shows the existence of Eulerian graphs embedded in surfaces that require knotted scaffolds for construction. The results presented can suggest, for instance, reconditioning of graphs to meet checkerboard colorability so that unknotted scaffold routings can potentially be found. In general, knot theory of non-intersecting Eulerian circuits is also of theoretical interest, as suggested in [24].

We note that, although the problem was motivated by DNA-origami scaffold routings, the results presented could be applied for any routing of a circular strand that can be modelled as a non-intersecting circuit in a surface-embedded graph. This is because a circuit in a

graph can be considered as an Eulerian circuit of a subgraph. The study of surface-embedded graphs significantly expands the systematic ways of designing nanostructures, and the study of the topology of circuits on such graphs can be a useful guide in the design of topologically complex 3D nanostructures.

References

1 Jaromir Abrham and Anton Kotzig. Construction of planar Eulerian multigraphs. In *Proc. Tenth Southeastern Conf. Comb., Graph Theory, and Computing*, pages 123–130, 1979.

2 Leonard M. Adleman. Molecular computation of solutions to combinatorial problems. *Science*, 266(5187):1021–1024, 1994. doi:10.1126/SCIENCE.7973651.

3 Mark A. Armstrong. *Basic Topology*. Springer New York, 1983.

4 Erik Benson, Abdulmelik Mohammed, Alessandro Bosco, Ana I. Teixeira, Pekka Orponen, and Björn Högberg. Computer-aided production of scaffolded DNA nanostructures from flat sheet meshes. *Angewandte Chemie International Edition*, 55(31):8869–8872, 2016. doi:10.1002/anie.201602446.

5 Erik Benson, Abdulmelik Mohammed, Johan Gardell, Sergej Masich, Eugen Czeizler, Pekka Orponen, and Björn Högberg. DNA rendering of polyhedral meshes at the nanoscale. *Nature*, 523(7561):441–444, 2015. doi:10.1038/nature14586.

6 Samuel W. Bent and Udi Manber. On non-intersecting Eulerian circuits. *Discrete Applied Mathematics*, 18(1):87–94, 1987. doi:10.1016/0166-218X(87)90045-X.

7 Dorothy Buck, Egor Dolzhenko, Nataša Jonoska, Masahico Saito, and Karin Valencia. Genus ranges of 4-regular rigid vertex graphs. *Electronic Journal of Combinatorics*, 22(3):P3.43, 2015.

8 Junghuei Chen and Nadrian C. Seeman. Synthesis from DNA of a molecule with the connectivity of a cube. *Nature*, 350(6319):631–633, 1991. doi:10.1038/350631a0.

9 Joanna A. Ellis-Monaghan, Greta Pangborn, Nadrian C. Seeman, Sam Blakeley, Conor Disher, Mary Falcigno, Brianna Healy, Ada Morse, Bharti Singh, and Melissa Westland. Design tools for reporter strands and DNA origami scaffold strands. *Theoretical Computer Science*, 671:69–78, 2017. doi:10.1016/j.tcs.2016.10.007.

10 Herbert Fleischner. *Eulerian Graphs and Related Topics. Part 1, Volume 1*, volume 45 of *Annals of Discrete Mathematics*. North-Holland Publishing Co., Amsterdam, 1990.

11 R. P. Goodman, I. A. T. Schaap, C. F. Tardin, C. M. Erben, R. M. Berry, C. F. Schmidt, and A. J. Turberfield. Rapid chiral assembly of rigid DNA building blocks for molecular nanofabrication. *Science*, 310(5754):1661–1665, 2005. doi:10.1126/science.1120367.

12 Jonathan L. Gross and Thomas W. Tucker. *Topological Graph Theory*. Dover Publications, INC, 2001. Dover reprint, original published in 1987.

13 Yu He, Tao Ye, Min Su, Chuan Zhang, Alexander E. Ribbe, Wen Jiang, and Chengde Mao. Hierarchical self-assembly of DNA into symmetric supramolecular polyhedra. *Nature*, 452(7184):198–201, 2008. doi:10.1038/nature06597.

14 Ryosuke Iinuma, Yonggang Ke, Ralf Jungmann, Thomas Schlichthaerle, Johannes B. Woehrstein, and Peng Yin. Polyhedra self-assembled from DNA tripods and characterized with 3D DNA-PAINT. *Science*, 344(6179):65–69, 2014. doi:10.1126/science.1250944.

15 Nataša Jonoska, Stephen A. Karl, and Masahico Saito. Creating 3-dimensional graph structures with DNA. In Harvey Rubin and David H. Wood, editors, *DNA Based Computers III*, volume 48 of *DIMACS Series in Discrete Mathematics and Theoretical Computer Science*, pages 123–136. AMS and DIMACS, 1999.

16 Nataša Jonoska and Masahico Saito. Boundary components of thickened graphs. In Nataša Jonoska and Nadrian C. Seeman, editors, *7th International Workshop on DNA-Based Computers*, volume 2340 of *Lecture Notes in Computer Science*, pages 70–81. Springer, 2001. doi:10.1007/3-540-48017-X_7.

17 Hyungmin Jun, Tyson R. Shepherd, Kaiming Zhang, William P. Bricker, Shanshan Li, Wah Chiu, and Mark Bathe. Automated sequence design of 3D polyhedral wireframe DNA origami with honeycomb edges. *ACS Nano*, 13(2):2083–2093, 2019. doi:10.1021/acsnano.8b08671.

18 Hyungmin Jun, Xiao Wang, William P. Bricker, and Mark Bathe. Automated sequence design of 2D wireframe DNA origami with honeycomb edges. *Nature Communications*, 10(5419):1–9, 2019. doi:10.1038/s41467-019-13457-y.

19 Hyungmin Jun, Fei Zhang, Tyson Shepherd, Sakul Ratanalert, Xiaodong Qi, Hao Yan, and Mark Bathe. Autonomously designed free-form 2D DNA origami. *Science Advances*, 5(1), 2019. doi:10.1126/sciadv.aav0655.

20 Vid Kočar, John S. Schreck, Slavko Čeru, Helena Gradišar, Nino Bašić, Tomaž Pisanski, Jonathan P. K. Doye, and Roman Jerala. Design principles for rapid folding of knotted DNA nanostructures. *Nature Communications*, 7:10803, 2016. doi:10.1038/ncomms10803.

21 Ajasja Ljubetič, Fabio Lapenta, Helena Gradišar, Igor Drobnak, Jana Aupič, Žiga Strmšek, Duško Lainšček, Iva Hafner-Bratkovič, Andreja Majerle, Nuša Krivec, Mojca Benčina, Tomaž Pisanski, Tanja Ćirković Veličković, Adam Round, José María Carazo, Roberto Melero, and Roman Jerala. Design of coiled-coil protein-origami cages that self-assemble in vitro and in vivo. *Nature Biotechnology*, 35(11):1094–1101, 2017. doi:10.1038/nbt.3994.

22 Abdulmelik Mohammed. *Algorithmic Design of Biomolecular Nanostructures*. PhD thesis, Aalto University, 2018.

23 Abdulmelik Mohammed and Mustafa Hajij. Unknotted strand routings of triangulated meshes. In Robert Brijder and Lulu Qian, editors, *DNA Computing and Molecular Programming*, volume 10467 of *Lecture Notes in Computer Science*, pages 46–63. Springer, 2017.

24 Ada Morse, William Adkisson, Jessica Greene, David Perry, Brenna Smith, Jo Ellis-Monaghan, and Greta Pangborn. DNA origami and unknotted A-trails in torus graphs. *arXiv preprint arXiv:1703.03799*, 2017. arXiv:/arxiv.org/pdf/1703.03799.pdf.

25 Dale Rolfsen. *Knots and Links*. AMS Chelsea Publishing, 2003. Reprint, original print in 1976.

26 Paul W. K. Rothemund. Folding DNA to create nanoscale shapes and patterns. *Nature*, 440(7082):297–302, 2006. doi:10.1038/nature04586.

27 Phiset Sa-Ardyen, Nataša Jonoska, and Nadrian C. Seeman. Self-assembling DNA graphs. *Natural Computing*, 2:427–438, 2003. doi:10.1023/B:NACO.0000006771.95566.34.

28 Nadrian C. Seeman. Nucleic-acid junctions and lattices. *Journal of Theoretical Biology*, 99(2):237–247, 1982. doi:10.1016/0022-5193(82)90002-9.

29 Nadrian C. Seeman and Neville R. Kallenbach. Design of immobile nucleic acid junctions. *Biophysical Journal*, 44(2):201–209, 1983. doi:10.1016/S0006-3495(83)84292-1.

30 William M. Shih, Joel D. Quispe, and Gerald F. Joyce. A 1.7-kilobase single-stranded DNA that folds into a nanoscale octahedron. *Nature*, 427(6975):618–621, 2004. doi:10.1038/nature02307.

31 Mu-Tsun Tsai and Douglas B. West. A new proof of 3-colorability of Eulerian triangulations. *Ars Mathematica Contemporanea*, 4(1):73–77, 2011.

32 Rémi Veneziano, Sakul Ratanalert, Kaiming Zhang, Fei Zhang, Hao Yan, Wah Chiu, and Mark Bathe. Designer nanoscale DNA assemblies programmed from the top down. *Science*, 352(6293):1534, 2016. doi:10.1126/science.aaf4388.

33 Gang Wu, Nataša Jonoska, and Nadrian C. Seeman. Construction of a DNA nano-object directly demonstrates computation. *Biosystems*, 98(2):80–84, 2009. doi:10.1016/j.biosystems.2009.07.004.